HYPERSONIC FLUTTER ANALYSIS BASED ON THREE-DIMENSIONAL LOCAL PISTON THEORY

Gaozhan Wang[1], Changchuan Xie[1,2*], Chenyu Liu[1], Chao An[1]

[1]School of Aeronautic Science and Engineering, Beihang University
Xueyuan Road 37, 100191, Beijing, China
wanggz@buaa.edu.cn
xiechangc@buaa.edu.cn
lcy@buaa.edu.cn
ac@buaa.edu.cn

[2]Hangzhou International Innovation Institute, Beihang University
166 Shuanghongqiao Street, Pingyao Town, Yuhang District, 311115, Hangzhou, China
xiechangc@buaa.edu.cn

Keywords: Flutter, aeroelasticity, hypersonic, local piston theory

Abstract: Hypersonic vehicle has become a research hotspot these years. Hypersonic vehicles' characteristics and working conditions led to special and significant aeroelastic flutter problems. Meanwhile, traditional flutter analysis methods are no longer suitable for super/hypersonic conditions. The local piston theory (LPT) is introduced and modified for the three-dimensional (3D) objects to express the unsteady aerodynamic force explicitly, and a tightly coupled state-space aeroelastic equation is derived. Then a hypersonic flutter analysis method is developed. A supersonic fin model with wind tunnel test results is used to verify the accuracy of this method. By comparing with wind tunnel test data, the effectiveness of the method is proved. This method can analyze 3D complex objects with both high accuracy and high efficiency, while suitable for high angle of attack (AOA) and wide Mach number range conditions.

1 INTRODUCTION

Hypersonic vehicle has great strategic significance and has become a research hotspot these years. Aeroelasticity represented by the flutter problem, due to its significant effect on flight safety, has become an essential aspect of aircraft design. As a fluid-structure interaction problem, aeroelasticity involves the interactions among aerodynamic, structural elastic, and inertial forces [1], for which the coupling mechanism is complex and difficult to analyze. Hypersonic vehicles often use a propulsion-airframe integrated design and often have a slender body layout with a thin-walled structure and lightweight materials [2], which leads to low structural stiffness and a propulsion-aeroelastic coupling problem. So, the effect of aeroelasticity on hypersonic vehicles is even more significant.

Traditional flutter analysis has formed a set of mature engineering methods, which can analyze the aeroelastic stability at zero and low angles of attack (AOAs) with high efficiency. However, super/hypersonic flutter analysis requires calculating the super/hypersonic unsteady aerodynamic

forces. Meanwhile, considering the operating condition of super/hypersonic vehicles, vehicle parts like fins and control surfaces may operate at high AOAs, which leads to the need for flutter analysis at high AOAs. For the reasons given above, traditional methods are no longer suitable, it is necessary to develop a new set of flutter analysis methods suitable for hypersonic conditions.

The basis of hypersonic flutter analysis is the calculation of supersonic unsteady aerodynamic forces. At present, commonly used calculation methods are mainly divided into computational fluid dynamics (CFD) methods and engineering methods. Computational fluid dynamics (CFD) is a numerical method directly solving either Euler equations or Navier-Stokes (N-S) equations, which can relatively truly reflect the physical nature of the flow [3], and allows for considering nonlinear effects such as viscous effect and shock wave interference. However, the CFD method has a significant computational complexity and low efficiency, making it almost impossible to use in practical aeroelastic engineering analysis [4]. Based on approximate unsteady aerodynamic models, engineering methods have high computational efficiency, but each method has a limited scope of application. At present, the widely used models including Newtonian impact theory [5], piston theory [6], shock–expansion theory [7], and lifting surface/panel approaches [8], are based on linear potential flow theory and the quasi-steady flow assumption, which generally suitable for low angles of attack (AOAs) conditions [9].

Piston theory has been widely used because of its simple form, high computational efficiency, and high accuracy in the applicable range [10]. Lighthill [6] first used piston theory to calculate the supersonic unsteady aerodynamic force. Ashley and Zartarian [11] discussed the application range of piston theory and proposed that piston theory can be used as a tool for aeroelasticity analysis. Doman, Oppenheimer, et al. [12,13] used first-order piston theory to establish an integrated dynamic model of air-breathing hypersonic vehicles.

To solve the problem of strict application preconditions of CPT, local piston theory (LPT) was developed. LPT ensures high computational precision，high efficiency, and a wider range of applications. In the 1950s, Morgan [14] first proposed the concept of LPT. In the 1990s, Chen et al. [15] used shock–expansion theory to calculate the local steady flow data and verified that LPT could still give a result with good accuracy under the condition of a thin airfoil with sharp leading edge and high AOA which the CPT already failed. Zhang et al. [16] used Euler-CFD-based LPT to analyze aeroelastic problems and extended the application range of LPT to the Mach number range 1.2-10. Meijer and Dala [10] presented a review of piston theory, including its theoretical foundation and subsequent developments.

At present, the related researches on the hypersonic flutter problem mainly focus on the analysis of two-dimensional (2D) airfoils and panels under low AOA conditions. Engineering methods and CFD methods are both widely used. Most researches using CFD methods are based on the full-order CFD-computational solid dynamics (CSD) coupling model. For researches using engineering methods, piston theory is mainly used. Chawla [17] used piston theory to study the flutter characteristics of an airfoil. Yates and Bennett [18] used shock–expansion–based LPT to carry out flutter analysis on the two-degree-of-freedom diamond airfoil. They also compared the results with the results carried out by Newtonian impact theory and strip theory. Ericsson et al. [19] analyzed the aerodynamic characteristics of an airfoil using the first-order LPT and compared results with wind tunnel test data. Yang [20] et al. used shock–expansion–based LPT to derive the aerodynamic

expression of a wing under high AOA conditions and analyzed the flutter characteristics of the wing.

It can be seen that the main limitation of hypersonic flutter analysis at present is the lack of efficient and high-precision analysis methods for special conditions such as three-dimensional (3D) objects and large AOAs. Based on the characteristic that the accuracy of LPT can be improved by combining with CFD or other high-precision steady aerodynamic force calculation methods, while still maintaining high efficiency, as well as being able to express the unsteady aerodynamic force in explicit form, this study carries out a 3D discretization form of LPT and establishes a state-space aerodynamic-structure tightly coupled model. Then a new hypersonic flutter analysis method based on three-dimensional local piston theory (3D-LPT) is developed, which is suitable for 3D complex objects under conditions with high AOA or wide Mach number range.

This paper is organized as follows: The establishment of flutter analysis framework, including CPT, LPT, 3D discretization form of LPT, aerodynamic-structure interface interpolation theory, and establishment of state-space flutter equation, is illustrated in Section 2. In Section 3, a supersonic fin model with wind tunnel test results is used to verify the accuracy of the method developed in this paper. The paper concludes in Section 4.

2   THEORY

Based on 3D discretized LPT and surface spline interpolation, the aerodynamic-structure tightly coupled state-space equation of the aeroelastic dynamic system is derived. Then based on Lyapunov's first method, the eigenvalues of the system characteristic matrix are used for system flutter stability analysis.

2.1   Classical and Local Piston Theories

Classical piston theory holds that the disturbance of one point on the aircraft body has little effect on other locations in the supersonic flow, so local pressure generated by the body's motion is related to the local normal component of fluid velocity in the same way that these quantities are related at the face of a piston moving in a one-dimensional channel [11], as shown in Figure 1. Then the wall pressure can be determined according to the isentropic assumption by the parameter of incoming freestream and the downwash velocity w.

$$p = p_\infty \left(1 + \frac{\gamma - 1}{2} \frac{w}{a_\infty} \right)^{\frac{2\gamma}{\gamma - 1}} \tag{1}$$

Equation (1) is the full-order formula of CPT, where p is the pressure on the aerodynamic surface, p_∞ is the pressure of the freestream, a_∞ is the sound speed of the freestream, γ is the ratio of specific heat, and w is the down-wash speed.
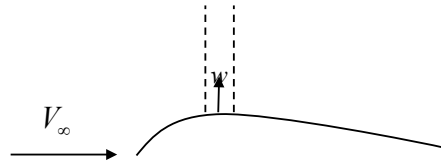
Figure 1: Illustration of CPT.

By excluding the higher order terms in the binomial expansion of the full order formula, the CPT formula with different precision can be obtained. First, second, and third-order formulas are commonly used. The first-order CPT formula is as follows:

$$p = p_\infty + \rho_\infty a_\infty w \tag{2}$$

where ρ_∞ denotes the density of the freestream.

The application preconditions of CPT are strict. Lighthill's original theory [6] states that $M_\infty^2 \gg 1$ needs to be satisfied, while the wall's motion speed needs to be less than the sound speed of the freestream. Therefore, CPT is only suitable for 2D thin airfoils with low AOA. CPT has a high calculation accuracy in the range of Mach number 2-5.

To solve the problem of strict application preconditions of CPT, LPT was developed. In LPT, freestream quantities (with subscript ∞) are replaced by the local flow quantities along the airfoil (with subscript L), and the down-wash speed W normal to the airfoil chord is replaced by the wash speed w_n normal to the wall created by wall's motion. The first-order LPT formula is as follows:
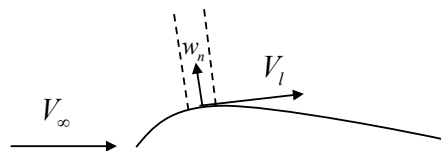
$$p = p_L + \rho_L a_L w_n \tag{3}$$

Figure 2: Illustration of LPT.

The essence of LPT is the dynamic linearization of the flow about a mean-steady-state [10]. Therefore, LPT can be combined with the high-precision CFD method, the steady flow field is calculated by CFD, while the unsteady part of aerodynamic force is calculated by piston theory, which realizes a better accuracy and a wider application range compared to CPT and other engineering methods, while the calculation efficiency is much higher than full CFD method. The application precondition of LPT is $M_\infty \tau_m \ll 1$, where τ_m denotes the dimensionless wall deflection caused by the wall's motion, which is generally easy to satisfy. So LPT breaks through the limitation of CPT that CPT is only suitable for thin wings with a small AOA, and extends the applicable range of piston theory.

4

2.2 3D Discretized Local Piston Theory

Although LPT has a wider applicable range than CPT, it is still only suitable for 2D objects, 3D effects in the flow field of complex objects cannot be considered. To consider the 3D effect, a 3D discretization form of LPT (3D-LPT) is carried out.

A local coordinate system is established to derive the normal wash speed of the wall in Equation (3) of an arbitrary point on the 3D aerodynamic surface. As shown in Figure 3, the origin of the coordinate o is the arbitrary point on the wall surface, the z_L axis is along the direction of the outer normal vector of the surface on that point, the x_L axis is along the direction of the local flow velocity V_L and the y_L axis is determined using the right-hand rule.
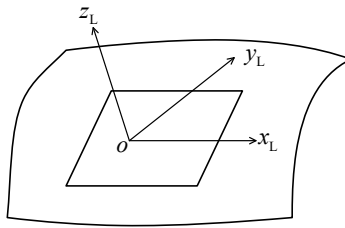

Figure 3: Local coordinate system on the wall surface.

In the body axis system *Oxyz*, the normal displacement of the arbitrary point caused by wall motion is defined as $u_L(x,y,t)$, then the normal wash speed of the wall consists of the time-dependent local velocity caused by wall motion, as well as the convective rate of displacement due to the surface gradient in the local flow direction, which is formulated as follows:

$$V_n = \frac{\partial}{\partial t} u_L + V_L \frac{\partial}{\partial x_L} u_L \tag{4}$$

where t is the time variable.

The displacement of the arbitrary point is defined as $w_P(x,y,z,t)$ in the body axis system, then the normal displacement can be expressed as:

$$u_L = \boldsymbol{n} \cdot \boldsymbol{w}_P = \boldsymbol{n}^T \boldsymbol{w}_P \tag{5}$$

where $\boldsymbol{n}$ is the outer unit normal vector of the surface on the arbitrary point.

By substituting Equation (5) into Equation (4), normal wash speed can be expressed as:

$$V_n = \boldsymbol{n}^T \left(\frac{\partial \boldsymbol{w}}{\partial t} + V_L \frac{\partial x}{\partial x_L} \frac{\partial \boldsymbol{w}}{\partial x} + V_L \frac{\partial y}{\partial x_L} \frac{\partial \boldsymbol{w}}{\partial y} + V_L \frac{\partial z}{\partial x_L} \frac{\partial \boldsymbol{w}}{\partial z} \right) \tag{6}$$

It's worth noting that, the local flow component V_{L} and the x_{L} axis are in the same direction, and thus $V_{\mathrm{L}} \cdot \dfrac{\partial x}{\partial x_{\mathrm{L}}}$ is the projection of V_{L} in the x directions of body axis system [21]. In the same way, $V_{\mathrm{L}} \cdot \dfrac{\partial y}{\partial x_{\mathrm{L}}}$ and $V_{\mathrm{L}} \cdot \dfrac{\partial z}{\partial x_{\mathrm{L}}}$ are the projections of V_{L} in the y and z directions, respectively.

Substituting the above transformation into equation (6), The wall element pressure formula of LPT applicable to arbitrary 3D aerodynamic surfaces is developed as follows:

$$p = p_{\mathrm{L}} + \rho_{\mathrm{L}} a_{\mathrm{L}} \boldsymbol{n}^{\mathrm{T}} \left(\frac{\partial \boldsymbol{w}}{\partial t} + V_{\mathrm{L}x} \frac{\partial \boldsymbol{w}}{\partial x} + V_{\mathrm{L}y} \frac{\partial \boldsymbol{w}}{\partial y} + V_{\mathrm{L}z} \frac{\partial \boldsymbol{w}}{\partial z} \right) \tag{7}$$

where the local flow quantities (with subscript L) are calculated by the Euler-based steady CFD analysis. $V_{\mathrm{L}x}$, $V_{\mathrm{L}y}$, and $V_{\mathrm{L}z}$ are the projections of V_{L} in the x, y, and z directions, respectively.

By modeling the body-fitted mesh for LPT based on the 3D geometry of the object, the discrete unsteady aerodynamic forces of the object can be expressed explicitly by using CFD and CSD analysis results.
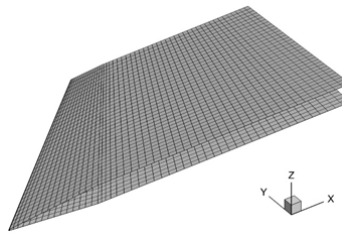

Figure 4: Body-fitted piston mesh for LPT of a fin model.

Mesh grid elements are taken as the calculation elements of 3D-LPT, and the physical quantities of the whole aerodynamic surface are assembled into matrix form based on the grid. The discretized pressure formula of 3D-LPT is derived as follows:

$$\mathbf{p} = \mathbf{p}_L + \boldsymbol{n}^{\mathrm{T}} \otimes \left(\mathbf{A}_{L1} \frac{\partial \boldsymbol{w}_p}{\partial t} + \mathbf{A}_{L2} \frac{\partial \boldsymbol{w}_p}{\partial x} + \mathbf{A}_{L3} \frac{\partial \boldsymbol{w}_p}{\partial y} + \mathbf{A}_{L4} \frac{\partial \boldsymbol{w}_p}{\partial z} \right) \tag{8}$$

where $\otimes$ refers to Hadamard product, $\mathbf{p}$ is the grid pressure vector, $\mathbf{p}_L$ is the grid local steady pressure vector, and is the grid normal vector matrix. $\mathbf{A}_{L1}$, $\mathbf{A}_{L2}$, $\mathbf{A}_{L3}$ and $\mathbf{A}_{L4}$ are local flow field parameter matrices from steady CFD analysis.

Once the pressure vector $\mathbf{p}$ is determined, the 3D-LPT aerodynamic force expression is obtained by integrating with the area of elements:

$$\mathbf{F}_P = \boldsymbol{n} \otimes \mathbf{S} \mathbf{p} \tag{9}$$

where $\mathbf{F}_P$ is the aerodynamic force vector, $\mathbf{S}$ is the grid area matrix.

2.3   High-dimensional Surface Spline Interpolation

Aeroelasticity is a typical fluid-structure interaction problem. For the 3D-LPT method in this study, it is necessary to transfer the flow field information obtained by CFD calculation and the modal information obtained by CSD calculation to the piston mesh. As shown in Figure 5, in most situations, the mesh of CFD and the mesh of CSD are mismatched on interfaces. High-dimensional Surface Spline Interpolation is exploited to exchange mechanical information such as deformations and loads between mismatched meshes.
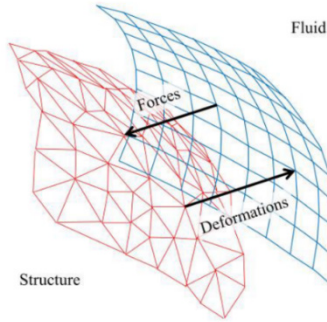

Figure 5 : Mismatched interface of the fluid domain and the solid domain.

The interpolation method widely used in aeroelastic analysis is the infinite plate spline (IPS) based on the analytical solution of elastic thin plates [22]. However, the traditional 2D interpolation method is not suitable for 3D objects with complex geometry. A high-dimensional surface spline interpolation method is introduced in this study [23].

Assume there are N-dimensional space vectors $\mathbf{X}_i$ with the number of n and the corresponding M-dimensional function values $\mathbf{W}_i$, as follows:

$$\begin{cases} \mathbf{X}_i = \begin{bmatrix} x^1 & x^2 & \ldots & x^N \end{bmatrix}_i^T \\ \mathbf{W}_i = \begin{bmatrix} w^1 & w^2 & \ldots & w^M \end{bmatrix}_i^T \end{cases} \quad i = 1, 2, \cdots, n \tag{10}$$

According to the IPS method, the following interpolation function can be established for each component w^p in $\mathbf{W}_i$:

$$w^p(\mathbf{X}) = c_0^p + \sum_{d=1}^{N} c_d^p x^d + \sum_{i=1}^{n} c_{N+i}^p r_i^2 \ln(r_i^2 + \varepsilon) \tag{11}$$

where $r_i^2 = \sum_{d=1}^{N} (x^d - x_i^d)^2$, $c_0^p, c_1^p, \cdots, c_{N+n}^p$ are the undetermined interpolation coefficients, ε is the given interpolation parameter, x_i^d is the D-th dimension coordinate of the i-th space vector.

To make the interpolation function satisfy the equation (10), the undetermined coefficients in equation (11) are determined by the following equations:

$$\begin{cases} \displaystyle\sum_{i=1}^{n} c_{N+i}^{p} = 0 \\[2mm] \displaystyle\sum_{i=1}^{n} c_{N+i}^{p} x_{i}^{d} = 0 \quad (d = 1, 2, \cdots, N) \\[2mm] c_{0}^{p} + \displaystyle\sum_{d=1}^{N} c_{d}^{p} x_{j}^{d} + \sum_{i=1,i\neq j}^{n} c_{N+i}^{p} r_{ji}^{2} \ln(r_{ji}^{2} + \varepsilon) + h_{j} c_{N+j}^{p} = w_{j}^{p} \quad (j = 1, 2, \cdots, n) \end{cases} \tag{12}$$

where $r_{ji}^{2} = \displaystyle\sum_{d=1}^{N} (x_{j}^{d} - x_{i}^{d})^{2}$, h_{j} is the weighting coefficient of the j-th space vector.

The coefficient matrix can be obtained by solving the equation (12), then the interpolation function (11) can be uniquely determined so that the function value of the arbitrary N-dimensional vector $\tilde{X}$ can be solved by the interpolation function.

The first partial derivative of the interpolation function is as follows:

$$\frac{\partial w^{p}}{\partial x^{d}} = c_{d}^{p} + 2\sum_{i=1}^{n} c_{N+i}^{p} \left[\ln(r_{i}^{2} + \varepsilon) + \frac{r_{i}^{2}}{r_{i}^{2} + \varepsilon} \right] (x^{d} - x_{i}^{d}) \quad (d = 1, 2, \cdots, N) \tag{13}$$

Based on the high-dimensional surface spline interpolation method, interpolation matrices G can be calculated from the parameters of CSD mesh, piston mesh, and CFD wall mesh. Then the displacement interpolation relationship between CSD wall mesh nodes and piston mesh element centroids and the flow field parameter interpolation relationship between CFD wall mesh nodes and piston mesh element centroids are established:

$$\begin{cases} \boldsymbol{w}_{P} = \boldsymbol{G}_{S} \boldsymbol{w}_{S} \\ \boldsymbol{\rho}_{p} = \boldsymbol{G}_{A} \boldsymbol{\rho}_{A} \\ \boldsymbol{a}_{p} = \boldsymbol{G}_{A} \boldsymbol{a}_{A} \\ \boldsymbol{V}_{p} = \boldsymbol{G}_{A} \boldsymbol{V}_{A} \end{cases} \tag{14}$$

where $\boldsymbol{w}$, $\boldsymbol{\rho}$, $\boldsymbol{a}$ and $\boldsymbol{V}$ are the displacement, local density, local sound speed, and local flow velocity matrix corresponding to each mesh. Subscript P represents the piston mesh element centroid, and subscripts S and A represent CSD mesh and CFD mesh nodes, respectively. $\boldsymbol{G}_{S}$ is the interpolation matrix between CSD wall mesh nodes and piston mesh element centroids, while $\boldsymbol{G}_{A}$ is the interpolation matrix between CFD wall mesh nodes and piston mesh element centroids.

For load interpolation between CSD wall mesh and piston mesh, it is necessary to satisfy the principle of virtual work, that is, there is equality between the virtual works of forces acting on the CSD and piston meshes.

According to the arbitrariness of virtual displacement, the load interpolation relation between the piston mesh and the CSD wall mesh can be deduced as follows:

$$\boldsymbol{F}_{\mathrm{S}} = \boldsymbol{G}_s^{\mathrm{T}} \boldsymbol{F}_P \tag{15}$$

The surface gradient of piston mesh $\dfrac{\partial \boldsymbol{w}_p}{\partial \mathbf{Q}}$ can also be obtained:

$$\frac{\partial \boldsymbol{w}_p}{\partial \mathbf{Q}} = \frac{\partial \mathbf{G}_s}{\partial \mathbf{Q}} \boldsymbol{w}_{\mathrm{S}} \tag{16}$$

where $\mathbf{Q} = \begin{bmatrix} x & y & z \end{bmatrix}^{\mathrm{T}}$ is the coordinate dimension matrix in the body axis system.

2.4 State-space aeroelastic vibration equation

Based on the structural dynamic model and the 3D-LPT aerodynamic model, the aeroelastic vibration equation of the system can be established. But first, it is necessary to derive the displacement of the wall surface $\boldsymbol{w}_S$ according to the structural dynamic model.

Employing the mode superposition method, the structural vibration displacement is discretized and described as a finite modal series:

$$\boldsymbol{w}_s = \boldsymbol{\Phi} \mathbf{q} \tag{17}$$

where $\boldsymbol{\Phi}$ and $\mathbf{q}$ are the free-vibration mode shapes and the generalized coordinates, respectively.

Then based on Lagrange's equations, the aeroelastic vibration equation can be established as follows:

$$\mathbf{M}\ddot{\mathbf{q}} + \mathbf{C}\dot{\mathbf{q}} + \mathbf{K}\mathbf{q} = \mathbf{F}_A\left(\dot{\mathbf{q}}, \mathbf{q}\right) \tag{18}$$

where $\mathbf{M}$, $\mathbf{C}$ and $\mathbf{K}$ are the generalized mass matrix, generalized damp matrix, and generalized stiffness matrix, respectively, and $\mathbf{F}_A\left(\dot{\mathbf{q}}, \mathbf{q}\right)$ denotes the generalized aerodynamic forces:

$$\mathbf{F}_A\left(\dot{\mathbf{q}}, \mathbf{q}\right) = \mathbf{F}_L + \mathbf{A}_0 \dot{\mathbf{q}} + \mathbf{A}_1 \mathbf{q} \tag{19}$$

where $\mathbf{F}_L$ is the local generalized aerodynamic force generated by the local steady pressure p_L, $\mathbf{A}_0$ and $\mathbf{A}_1$ are the generalized aerodynamic influence coefficient (AIC) matrices derived by 3D-LPT.

Then, combined with equation (18) and equation (19), the aerodynamic-structure tightly coupled vibration equation of the aeroelastic dynamic system is derived in state-space form as follows:

$$\dot{X} = AX + B \tag{20}$$

where $X = \begin{bmatrix} \dot{q} \\ q \end{bmatrix}$, $A = \begin{bmatrix} M^{-1}(A_0 - C) & M^{-1}(A_1 - K) \\ I & 0 \end{bmatrix}$, $B = \begin{bmatrix} M^{-1}F_L \\ 0 \end{bmatrix}$, I and 0 are the identity matrix and the zero matrix, respectively.

2.5 Flutter analysis based on linear system stability theory

The aeroelastic stability of the system is discussed based on the aeroelastic equation (20). In engineering applications, the stability analysis of dynamic systems is usually to analyze the exponential stability of the dynamic solution after the equilibrium solution of the system is disturbed. Based on Lyapunov's first method, the eigenvalue of the system characteristic matrix is used to judge the stability of the system，which is a widely used method to analyze the dynamic stability of linear systems.

For the dynamic system described by equation (20), the sufficient and necessary condition for its equilibrium solution to be exponentially stable is that all eigenvalues of the characteristic matrix A have negative real parts, otherwise, the system is unstable and flutter may occur.

The damping coefficient (the real part of the eigenvalue divided by the imaginary part of the eigenvalue) and the oscillation frequency (the imaginary part of the eigenvalue divided by 2π) can be calculated from the eigenvalue of the characteristic matrix A. Then the curves of damping coefficient and vibration frequency with velocity can be drawn, that is, the V-g and V-f curves, and the flutter velocity is determined by finding the crossing point of the V-g curve.

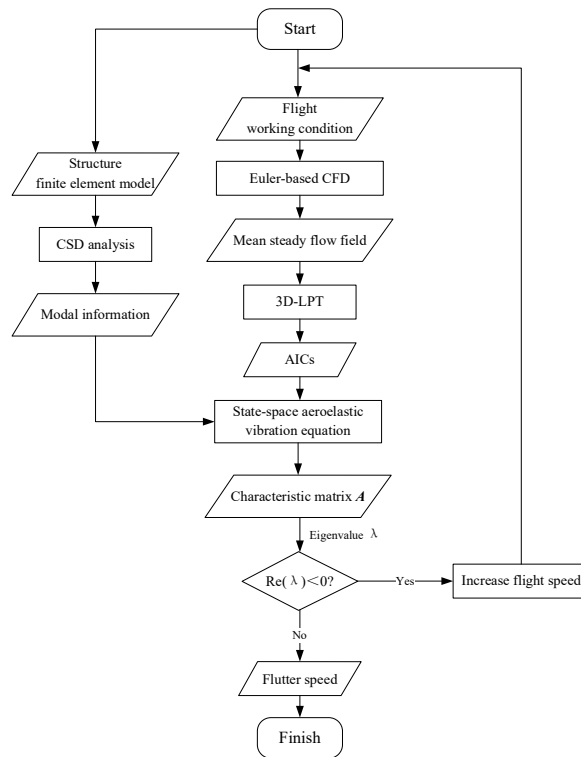In summary, the flow of the flutter analysis method proposed in this study is shown in Figure 6.

Figure 6：Scheme of the state-space flutter analysis using 3D-LPT.

Because only one steady CFD calculation is needed for the same flow velocity condition, CFD iteration is avoided and the calculation amount is greatly reduced.

3   EXPERIMENTAL VERIFICATION

A supersonic fin model with wind tunnel test results is used to verify the accuracy of the flutter analysis method proposed in this study.

3.1   Test model

As shown in Figure 7, the test fin model consists of a trapezoidal fin body and a shaft. The trapezoidal body has a small thickness in the top and considerable thickness in the root, and the fin shaft is a rectangular section beam. The main structure of the fin model is made of aluminum alloy, while the material of the fin shaft is steel. The root of the shaft is fixed onto a rigid support.
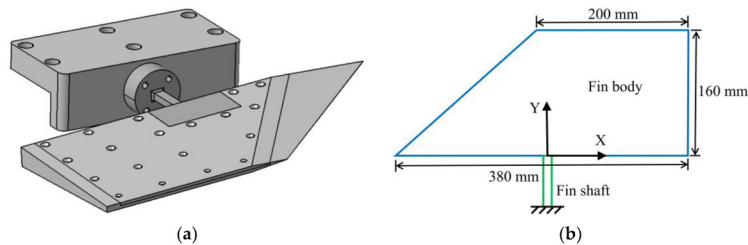

Figure 7：Test fin: (a) Configuration; (b) Geometric dimension.

3.2   Structural dynamic analysis

The commercial software MSC.NASTRAN was used for CSD modal analysis of the fin's finite element model. The modal shape of each order and the corresponding generalized mass and stiffness data were obtained through CSD analysis. To ensure the accuracy of the analysis results, the CSD analysis results of the first order (first torsion) and the third order (first bending) are compared with the hammering method modal test results of the real model as shown in Figure 8, and the finite element model is modified according to the test results. The comparisons between the modified CSD results and the test results of first-order and third-order modes are shown in Table 1, and the corresponding modal shapes are shown in Figure 9. The comparison results show that the modified finite element model is valid in simulating the dynamic characteristics of the real model and is capable of the following aeroelastic analysis.
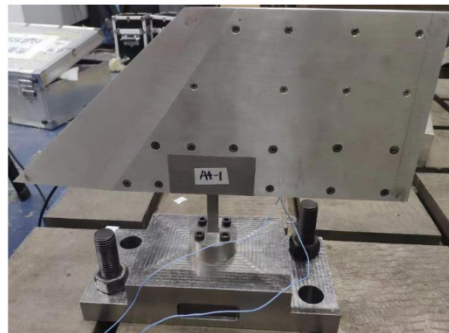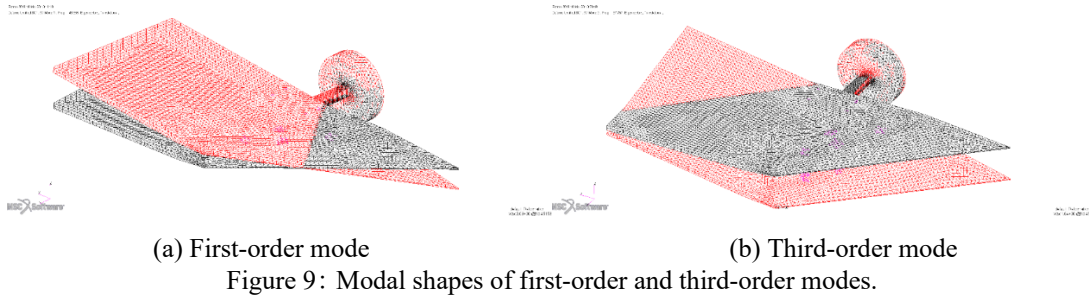

Figure 8：Real model vibration test.

Table 1: Comparisons between the modified CSD results and the test results.

Order	Frequency (Hz)		Error
	Test	CSD	
1(First torsion)	48.8	48.855	0.11%
3(First bending）	67.8	67.767	-0.05%

(a) First-order mode   (b) Third-order mode
Figure 9: Modal shapes of first-order and third-order modes.

3.3 Wind tunnel flutter test

An intermittent transonic and supersonic wind tunnel with a section size of 0.6m×0.6m was used for the flutter test. Wind tunnel tests were conducted at four AOA conditions of 4°, 6°, 8°, 10°. Under each working condition, the Mach number of the incoming flow was fixed at 2.5, and the dynamic pressure of the incoming flow increased continuously from low to high until the flutter occurred. The wind tunnel test scene is shown in Figure 10.

Figure 10: Wind tunnel test scene.

The flutter dynamic pressures and flutter frequencies at different AOAs were obtained by wind tunnel tests, and the corresponding equivalent flutter velocities were converted from flutter dynamic pressures using the air density at sea level. The wind tunnel test results are listed in Table 2.

Table 2: Flutter results of the wind tunnel tests.

AOA (deg)	Flutter Frequency (Hz)	Flutter Dynamic Pressure (kPa)	Equivalent Flutter Speed (m/s)
4	58.5	76.8	354.10
6	58.9	71.7	342.14
8	60	69.2	336.12
10	60	67.2	331.23

It can be seen from the test results that with the increase of AOA, the flutter speed decreases while the flutter frequency is basically unchanged.

3.4 3D-LPT flutter analysis

3.4.1 Euler-CFD calculation

Commercial software ANSYS-Fluent was used for CFD calculation. The density-based solver with an implicit formulation was used and the air in the flow field was modeled as the ideal gas. The boundary conditions were similar to the wind tunnel test. The CFD mesh and flow field are shown in Figure 11.
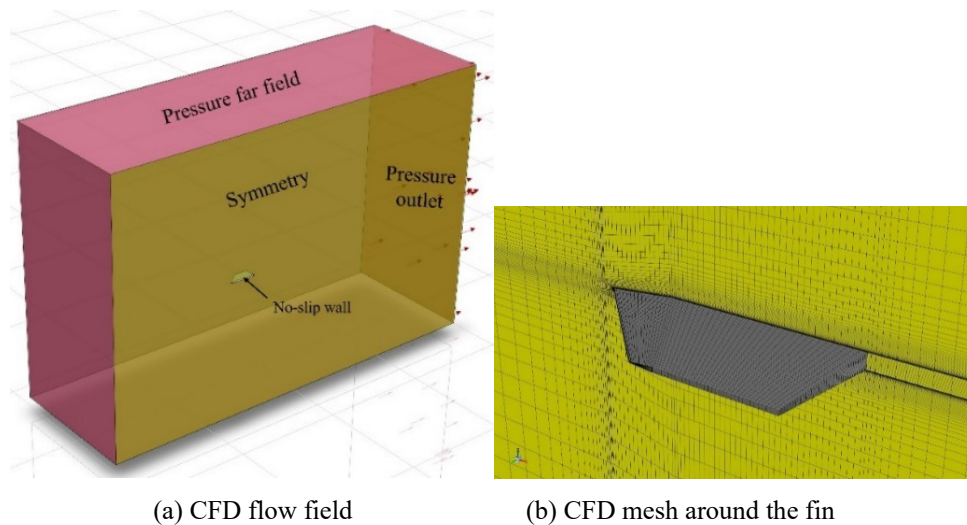
(a) CFD flow field   (b) CFD mesh around the fin
Figure 11 : Computational domain and mesh of the CFD model.

The CFD calculation conditions were consistent with the wind tunnel test. Under all calculation conditions, continuity, velocity, and energy residuals can be reduced to below 10^{-7}, which proved that CFD calculation achieved a good convergence.

As there are many calculation conditions, only one steady CFD result is shown here. The absolute pressure cloud diagram of the condition with 6° AOA and 70kPa incoming flow dynamic pressure is shown in Figure 12.
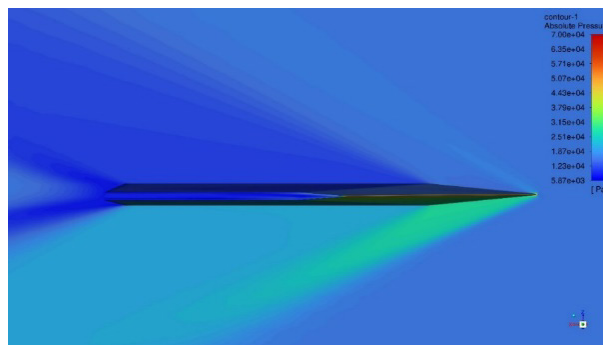

Figure 12 : Absolute pressure cloud diagram (6°, 70kPa).

3.4.2 Euler-CFD calculation

Based on the steady Euler-CFD results of each working condition, the flutter analysis process described in Section 2.5 was adopted to calculate the eigenvalues, corresponding damping coefficients, and oscillation frequencies under a series of dynamic pressure values for the working conditions of 4°, 6°, 8°, and 10° AOA, respectively. Finally, the root locus, flutter dynamic pressure, and V-g and V-f curves under different AOA conditions were obtained. According to the results, the crossing mode is the third-order mode, and the coupled modes are the first-order and third-order modes for every AOA condition.

As there are many calculation conditions, only the results of the 6° AOA condition are shown here. As shown in Figure 13, with an increasing dynamic pressure, the eigenvalue of the third-order mode (first bending) gradually moves towards the positive real-axis direction in the root locus and crosses the zero real axis when the dynamic pressure increases to 72.28kpa, wherein the critical crossing point indicates the flutter boundary. When the eigenvalue crosses the zero real axis, it can be seen in the V-g curve that the damping coefficient of the third-order mode changed from negative to positive, while the corresponding flutter frequency in the V-f curve was 59.34Hz.
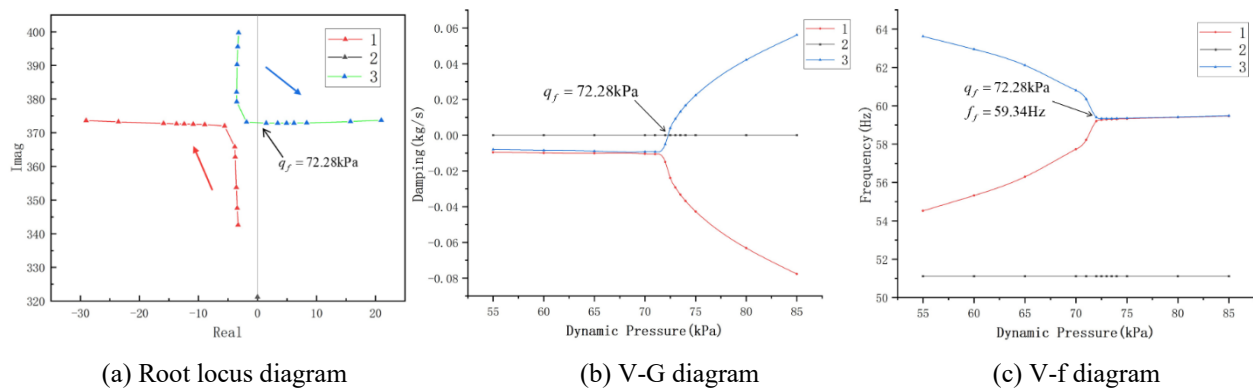

| (a) Root locus diagram | (b) V-G diagram | (c) V-f diagram |

Figure 13 : Flutter diagrams of 6° AOA condition.

The flutter results for 3D-LPT at all AOAs and the comparison with the test results are listed in Table 3. In comparison to the wind tunnel test results, the 3D-LPT method has a high analysis accuracy for flutter velocity and flutter frequency, with errors less than 4% and 1.5%, respectively.

Table 3 : Flutter results and comparison.

AOA (deg)	Flutter Frequency (Hz)		Error	Flutter Dynamic Pressure (kPa)		Error	Equivalent Flutter Speed(m/s)		Error
	3D-LPT	Test		3D-LPT	Test		3D-LPT	Test	
4	59.36	58.5	1.47%	72.63	76.8	-5.43%	344.35	354.10	-2.75%
6	59.34	58.9	0.75%	72.28	71.7	0.81%	343.52	342.14	0.40%
8	59.38	60	-1.03%	72.27	69.2	4.44%	343.50	336.12	2.19%
10	59.44	60	-0.93%	72.19	67.2	7.43%	343.31	331.23	3.65%

3.5 3D-LPT flutter analysis

Comparisons of the flutter speeds and frequencies using different methods are shown in Figure 14.
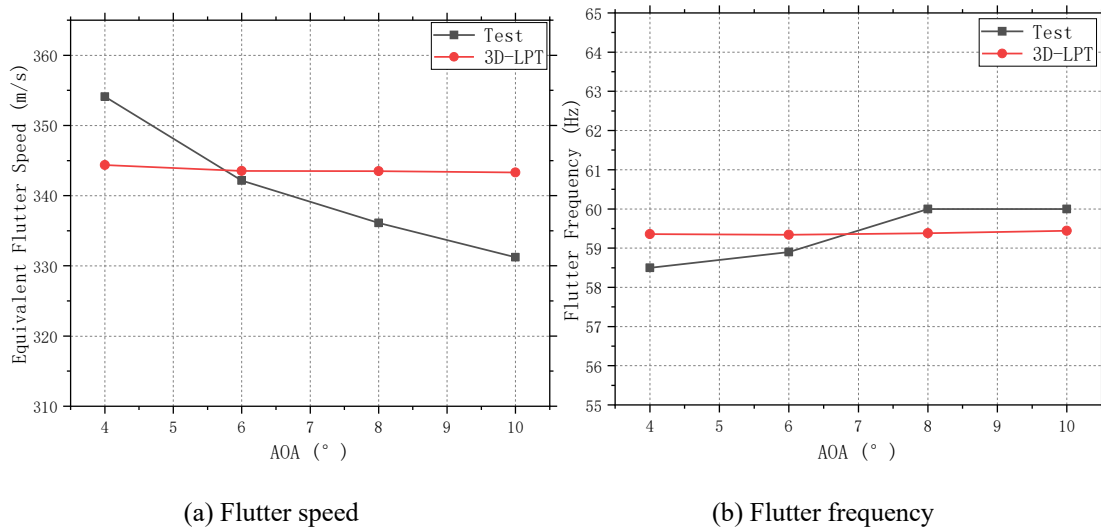
(a) Flutter speed (b) Flutter frequency

Figure 14: Flutter results comparisons.

The flutter results of 3D-LPT are in good agreement with the wind tunnel test results under multiple AOA conditions ranging from 4° to 10°, which preliminarily proves the effectiveness of this method and its applicability for supersonic flutter analysis under high AOA conditions.

With increasing AOA, the variations in flutter frequencies and the relative errors in the flutter frequencies between 3D-LPT results and test results are negligible.

There is an obvious decreasing trend in the test flutter speed with increasing AOA. However, the reduction in 3D-LPT flutter speed is limited. Therefore, the flutter velocity error of 3D-LPT decreases first and then increases as AOA increases. Because the non-viscous model based on the Euler equation is used in steady CFD calculation, the viscous nonlinear effect caused by the increase of AOA cannot be considered, which can be one of the possible causes for this error since the precision of the LPT significantly depends on the accuracy of the steady flow results

4 CONCLUSIONS

In this research, a hypersonic flutter analysis method based on three-dimensional local piston theory(3D-LPT) is developed. A supersonic fin model with wind tunnel test results is used to verify the accuracy of this method. Our primary achievements and conclusions are as follows:

1) Euler-based CFD is used to calculate the steady flow field of LPT. And the LPT is extended by 3D discretization. Then a super/hypersonic unsteady aerodynamic calculation method based on 3D-LPT is established. This method significantly improved the accuracy of piston theory and expanded its application range while still maintaining a high efficiency, and being able to express the unsteady aerodynamic force in explicit form. The 3D-LPT method is suitable for 3D complex objects under conditions with high AOA or wide Mach number range.

2) Based on the unsteady aerodynamic force expression in explicit form carried out by 3D-LPT and the high-dimensional surface spline interpolation method, a state-space aerodynamic-structure tightly coupled model is established. A flutter analysis method based on eigenvalues of the system characteristic matrix is also established according to the linear system stability

15

theory. Since 3D-LPT is able to express the unsteady aerodynamic force in a small disturbance range explicitly just with the steady CFD calculation data, a tightly coupled state-space equation can be established, which can be directly solved. Compared with the full-order CFD-CSD coupled analysis method, CFD iteration is avoided and the calculation amount is greatly reduced.

3) By analyzing a supersonic fin model with the 3D-LPT method, and comparing the results with the wind tunnel data, the effectiveness of this method is proved. Under the condition of Mach number 2.5, the flutter equivalent velocities and flutter frequencies of the fin model with 4°, 6°, 8°, and 10° AOAs were calculated. In comparison to the wind tunnel test results, the errors were less than 4% and 1.5%, respectively. The comparison results show that the 3D-LPT results are in good agreement with the wind tunnel test results, which can prove the effectiveness of this method, and its applicability for supersonic flutter analysis under high AOA conditions.

4) According to the wind tunnel test results, there is an obvious decreasing trend in the test flutter speed with increasing AOA, while the flutter frequency is basically unchanged. However, the decreasing trend of flutter velocities obtained by 3D-LPT is not obvious. A possible cause for this error may be the viscous nonlinear effect caused by the increase of AOA, which cannot be considered in Euler-based CFD. Since the precision of the LPT significantly depends on the accuracy of the steady flow results, how to consider the nonlinear effects such as viscosity is the key and further research direction to improve the analytical accuracy of this 3D-LPT-based flutter analysis method.

REFERENCES

[1] Hodges, D.H.; Pierce, G.A. Introduction to Structural Dynamics and Aeroelasticity, 2nd ed.; Cambridge University Press: Cambridge, UK, 2011; pp. 1–247.

[2] YANG C, XU Y, XIE C C. Review of studies on aeroelasticity of hypersonic vehicles[J]. Acta Aeronautica et Astronautica Sinica, 2010, 31(1): 1-11(in Chinese).

[3] YE Z Y, MENG X Z, LIU C, et al. Progress and prospects on aeroelasticity of hypersonic vehicles[J]. Acta Aerodynamica Sinica, 2018,36(06):984-994(in Chinese).

[4] Schuster D M, Liu D D, Huttsell L J .Computational Aeroelasticity: Success, Progress, Challenge[J].Journal of aircraft, 2003(5):40.

[5] XU Y. Studies on aeroelasticity of hypersonic vehicles[D]. Beijing: Beihang University, 2008 (in Chinese).

[6] Lighthill M J. Oscillating airfoils at high Mach number[J].Journal of the Aeronautical Sciences, 1953, 20(6):402-406.DOI:10.2514/8.2657.

[7] Jones JG. Shock-expansion theory and simple wave perturbation. Journal of Fluid Mechanics. 1963;17(4):506-512. DOI:10.1017/S0022112063001488

[8] Chen P C, Liu D D. Unified hypersonic/supersonic panel method for aeroelastic applications to arbitrary bodies[J]. Journal of Aircraft, 2015, 39(3):499-506. DOI:10.2514/2.2956.

[9]   Mcnamara J J, Friedmann P P. Aeroelastic and Aerothermoelastic Analysis in Hypersonic Flow: Past, Present, and Future[J].AIAA Journal, 2011, 49(6):1089-1122.DOI:10.2514/1.J050882.

[10]   Meijer, Marius-Corné, Dala, et al. Generalized Formulation and Review of Piston Theory for Airfoils[J]. AIAA Journal, 2016, 54(1):17-27. DOI:10.2514/1.J054090.

[11]   Ashley H, Zortarian G. Piston theory a new aerodynamic tool for the aeroelastician[J]. Journal of the Aeronautical Sciences, 1956, 23(12):1109-1118. DOI:10.2514/8.3740.

[12]   Oppenheimer M, Doman D. A Hypersonic Vehicle Model Developed With Piston Theory[C]// AIAA Atmospheric Flight Mechanics Conference and Exhibit. 2006.

[13]   Bolender M, Oppenheimer M, D Doman. Effects of Unsteady and Viscous Aerodynamics on the Dynamics of a Flexible Air-breathing Hypersonic Vehicle[C]// Aiaa Atmospheric Flight Mechanics Conference & Exhibit. 2007.

[14]   Morgan H, Runyan H, Huckel V. Theoretical Considerations of Flutter at High Mach Numbers[J].Journal of the Aerospace Sciences, 1958, 25(6):371-381. DOI:10.2514/8.7688.

[15]   CHEN J S, CAO J. An approximate calculating method of supersonic/hypersonic unsteady aerodynamic forces of airfoils[J]. Acta Aerodynamica Sinica, 1990, 8(3): 339-344 (in Chinese).

[16]   Zhang W W, Ye Z Y. Numerical Method of Aeroelasticity Based on Local Pistion Theor [J].Chinese Journal of Theoretical and Applied Mechanics ,2005,(05):632-639 (in Chinese).

[17]   Chawla J P .Aeroelastic instability at high mach number[J].Journal of the Aerospace Sciences, 1958, 25(4):246-258. DOI:10.1016/S0083-6729(08)60513-0.

[18]   Yates E.C., Bennett R.M. Analysis of Supersonic-Hypersonic Flutter of Lifting Surfaces at Angle of Attack[J]. Journal of Aircraft, 1972, 9(7): 481-489

[19]   Ericsson L.E. Viscous and Elastic Perturbation Effects on Hypersonic Unsteady Airfoil Aerodynamics[J]. AIAA Journal, 1977, 15(10): 1481-1490

[20]   Yang B Y, Song W L. Supersonic Flutter Calculation of a Wing with Attack Angle by Local Flow Pistion Theory [J]. Journal of Vibration and Shock, 1995(02):60-63+81 (in Chinese).

[21]   Liu, C.; Xie, C.; Meng, Y.; Bai, L. Experimental and Numerical Flutter Analysis Using Local Piston Theory with Viscous Correction. Aerospace 2023, 10, 870. https://doi.org/10.3390/aerospace10100870

[22]   Johnson E.H., Rodden W.P. MSC/NASTRAN Aeroelastic Analysis User's Guide[M]. 68th ed. CA, USA: The MacNeal-Schwendler Corporation Publication, 1994

[23]   Xie C , Yang C . Surface Splines Generalization and Large Deflection Interpolation[J].Journal of Aircraft, 2007.DOI:10.2514/1.24571.

COPYRIGHT STATEMENT